Proceedings of Ninth World Conference on Earthquake Engineering
August 2-9, 1988, Tokyo-Kyoto, JAPAN (Vol.VIII)

SG-9

UNBONDED POST-TENSIONED DUCTILE MOMENT RESISTANT FRAMES

Neil M. HAWKINS[1] and Takayuki ISHIZUKA[2]

[1]Department of Civil Engineering, University of Washington, Seattle, WA., U.S.A.
[2]Shimizu Construction Company, Chuo-ku, Tokyo, Japan

SUMMARY

Results are described of high intensity reversed cyclic loading tests on three exterior column-beam subassemblages. In two, the beams contained unbonded post-tensioning tendons, and, in one, the beam's deformed bar reinforcement was improperly anchored in the connection. Limited prestress did not adversely affect the subassemblages' seismic response. These results were used to introduce into the U.S.A.'s NEHRP provisions, regulations for post-tensioning of ductile moment resisting frames (Ref. 1).

INTRODUCTION

Reference 2 prohibits the use of prestressing tendons to resist seismic forces in ductile moment resisting frames. Forces must be carried entirely by reinforcement with a yield strength not greater than 60,000 psi. Yet tendons may be desirable for deflection control purposes, or for the assembly of frames from precast elements. To examine the seismic performance of exterior column-partially prestressed beam connections, three subassemblages were tested (Ref. 3). Details are shown in Figs. 1 and 2. The FS specimen simulated, to full-scale, conditions in a ductile frame building in Seattle. The RC and PPC specimens were approximately two-third scale models of the FS specimen. The beams of the FS and PPC specimens were partially prestressed with unbonded tendons.

FS SPECIMEN

Materials Shown in Fig 2(a) are the reinforcements for the longitudinal beam of the FS specimen. Amounts, lengths and bend points duplicated the same quantities for the exterior column-beam connection of the existing building. The tendons caused an average prestress, with respect to the beam's rectangular section, of 312 psi. Yield stresses were 60 and 76 ksi for the No. 9 and No. 11 bars, respectively. Grade 270 steel was used for the unbonded tendons. Concrete strengths at test were 5,880 psi for the beam and 5,750 psi for the column.

Unconventional reinforcing details were the use of unbonded tendons; the turning up of the longitudinal beam's top bars at the front face of the column; and not terminating the bottom bars with standard 90 degree hooks.

Test Arrangement The column ends were pinned at the mid-height of the columns in the building, and subjected by a testing machine to an axial compressive force

of 755 kips. Deformations were measured for the beam's plastic hinge zone; the beam's tip; the column and the column joint; and strains for two of the longitudinal beam's top bars and two of its bottom bars. To simulate gravity effects, a constant 43.2 kip load was applied to the beam at 38 inches from the beam-column interface. A reversing load, that simulated earthquake effects, was applied 202.5 inches from the column face.

Loadings were two major cycles between the desired displacement limits, followed by one minor cycle between displacements of ± 1/2 inch. Between sequences, the major cycle limits were incremented initially by one-half or, later, by one inch until tip displacements reached ± 8 inches. That displacement equalled a 4% inter-story drift or twice the maximum desirable displacement. The loading rig was unable to accommodate larger displacements.

Results The specimen had not failed and its strength was still increasing when loading stopped. There was no evidence of an impending bond or a shear failure. During displacements to ± 3.5 inches, the column surface immediately above the beam spalled. However, the spalling was minimal and did not increase in later cycles to greater displacements.

Shown in Fig. 3 is the specimen's equivalent tip load-tip displacement relationship. The gravity load, the beam's self-weight and the loading devices caused moments at the column face. Thus, ordinates in Fig. 3 are the load which, when acting at the beam's tip, caused the same total moment at the column face as that acting on the specimen. Although the strength of the specimen was still increasing with increasing displacements when testing was stopped, it is clear from Fig.3 that the beam reached its plastic collapse capacity. Even at large displacements, the hysteretic loops were stable and without pinching effects. Bond deterioration within the connection must have been minimal in spite of the inadequate anchorage conditions for the beam bars. However, the moment-curvature relationship for large displacements was unusual. The unbroken line in Fig. 4 is the observed relationship for the last loading cycle. Curvatures are averages measured over 24 inches from the column face. Moments are those for the mid-point of that length. The energy dissipated for upward loading is good, but that for downward loading is not. The broken line shows the result predicted by computer modeling (Ref. 4). The two relationships agree reasonably well, but show characteristics undesirable for ductile moment resisting frames.

Except for unfavorable energy dissipation for downward loading, and in spite of poor anchorage for the beam bars, this FS specimen performed acceptably. Undoubtedly, that was due to the prestress.

RC AND PPC SPECIMENS

Materials Because of the favorable result for the FS specimen, the behavior of subassemblages without (RC) and with prestress (PPC) was compared directly. The RC specimen was designed according to ACI requirements (Refs. 5, 6).

Figure 2 shows reinforcement details for the RC and PPC beams. Both had 2-#8 bars top and bottom. The PPC specimen was also prestressed with three unbonded 1/2 inch Grade 270 seven-wire strands located at the center of gravity of the T-section. The average prestress for that beam's rectangular cross section was 330 psi. The RC specimen had 8-#3 bars extending from the spandrel beam into the slab, and the PPC specimen had 8-#2 bars, so that the downward loading strengths for the two beams were almost the same. While main bars were anchored in the connection as required by Reference (5), that condition was theoretically more critical than shear or flexural conditions for the beam, the connection, or the columns. Concrete compressive strengths were 4,050 and 4,190 psi for the RC and PPC specimens, respectively. Yield strengths were 64.9, 67.5,

and 62.3 ksi for the #2, 3 and 8 bars, respectively. For the prestressing steel, the yield and ultimate strengths were 247.8 and 275.8 ksi, respectively.

Test Arrangements The test set-ups for both specimens were essentially the same as that for the FS specimen. A constant axial load of 140 kips was applied to the column, constant vertical loads of 20 kips, were applied to the tips of the spandrel beams, and a cyclically reversing, displacement-controlled, tip load was applied to the beam at 70 inches from the column face. Loading sequences consisted of four elastic cycles of increasing magnitude followed by two cycles that caused yielding of the beam's bars at the column face for both downward and upward loading. Those cycles established a yield displacement, δy, defined as the tip displacement at the beam bars' first yield. For subsequent cycles, limiting displacements were incremented by δy and the loading described in terms of the displacement ductility factor, DDF, where DDF was the tip displacement divided by δy. After DDFs of one, two, four, and seven, small magnitude cycles were inserted to examine aftershock response.

Results Diagonal cracks on the side-faces of the longitudinal beam were more marked for both specimens than for the FS specimen.At a given cycle, the number of cracks, both flexural and shear, were larger for the RC than for the PPC specimen. For the RC specimen, crushing of the beam's cover at the bottom face adjacent to the column started at a DDF of 4. However, spalling was minimal even by the end of the test. For the PPC specimen, spalling first occurred at a DDF of 2. That DDF was less than for the RC specimen because the prestress altered the strain distribution. That concrete spalled off at a DDF of 4 and the extent of the spalling increased with cycling until the test ended at a DDF of 10. For the RC specimen, relatively wide cracks developed from where the diagonal edge of the slab intersected the longitudinal beam's stem. Those cracks spread along the beam-slab interface and affected T-beam action for both shear and flexure. For the PPC specimen, those cracks were not marked.

Shown in Fig. 5 are tip load-tip displacement relationships. For both specimens, hysteretic loops were stable with no evidence of severe damage, even for a DDF of 8. However, because of concrete crushing at a DDF of 2 in the PPC specimen, strengths for downward loading became constant earlier for the PPC than for the RC specimen. At a DDF of 4, loops for the RC specimen were only slightly fatter than those for the PPC specimen. For small cycles following large DDF values, the PPC specimen was 50 percent stiffer than the RC specimen.

DISCUSSION

Moment Index Hysteretic loops are affected by many parameters. However, the basic shape is determined by the flexural properties of the beam. Flexural properties are best compared using a "moment index" concept. For the section shown in Fig. 6, appropriate moment indices for ordinary, μ_w, and prestressing steel, μ_{pw}, can be calculated as shown in Table 1, where f_{ps} is the prestressing steel's nominal strength, f'_c is the concrete strength and f_y is the yield stress for A_s. Quantities μ_w and μ_{pw} represent the relative contributions of ordinary and prestressing steel, respectively, to the flexural strength. The index $\mu_w/(\mu_w+\mu_{pw})$, reflects the dependency of flexural strength on prestressing steel. For an index of 1.0, the section is reinforced concrete only. As the index decreases, the strength is increasingly dependent on the prestressing steel.

Indices for the beams of the three subassemblages are listed in Table 1. For the FS specimen, slab steel located within a width of 80 inches was considered effective as negative steel, based on the measured strains. For the RC and PPC specimens, all slab steel was considered effective. Prestressing steel was considered as both negative and positive reinforcement. For the FS and PPC specimens, 75 and 65%, respectively, of the strengths for downward loading

were contributed by ordinary reinforcement (row 4). The indices in rows 1 through 8 are not unusual and indicate no obvious reason for the irregular moment-curvature relationship for the FS specimen. Ratios of the moment indices ($\mu_w + \mu_{pw}$) for upward and downward loading are listed in row 9. The FS specimen ratio is significantly smaller than the RC and PPC ratios. Further studies of that effect and of prestress were made analytically (Ref. 3).

Bottom to Top Steel Ratio Shown in Fig. 7 are predictions of the effects of the A'_s/A_s ratio. Top reinforcement was held constant at 2.37 in^2. The peak curvature value of $\pm$ 0.001 radian/inch is that for a DDF of 3 for the RC specimen. The loop for Case 1 is an almost perfect spindle. Yet that shape becomes increasingly distorted, with decreasing energy dissipation for downward loading as the A'_s/A_s ratio decreases. The loop for Case 3 is similar to that for the FS specimen. For a section with the A'_s/A_s less than about 0.65 the top steel yields in tension but not in compression. Tensile strains accumulate and lengthen that reinforcement, and the top flexural cracks never close. The bottom steel undergoes large reversing strains, subjecting it to worse bond conditions than for a symmetrically reinforced section.

Prestress Effect Shown in Fig. 8 are predicted moment-curvature relationships for the RC and PPC specimens. The ratio A'_s/A_s was taken as 0.64 and, hence, the loop for the RC specimen is similar to that for Case 2 in Fig. 7. Broken lines show where concrete contributes to flexural strength. For the RC specimen, that contribution occurs only for downward loading. However, with prestressing, flexural cracks close for both loading directions so that the loop for the PPC specimen is slightly thinner, close to zero load, than that for the RC specimen. Nevertheless, the total energy dissipation is greater for the PPC specimen. But, as the prestress increases, loops become thinner, and the energy dissipation becomes less than for an RC specimen. Further, if the prestress is located optimally for gravity load, it is difficult to maintain the ($\mu_w+\mu_{pw}$) ratio for the bottom steel greater than 0.65 that for the top steel.

CONCLUSIONS

Limited amounts of prestress do not adversely affect the response of ductile moment resisting frames. The nominal average prestress, based on the beam's rectangular cross-sectional area, should not exceed about 350 psi; the index $\mu_w/(\mu_w+\mu_{pw})$ should equal or exceed 0.65 for both upward and downward loadings; and the ratio ($\mu_w+\mu_{pw}$) for the bottom reinforcement to ($\mu_w+\mu_{pw}$) for the top reinforcement should also equal or exceed 0.65.

REFERENCES

[1] Building Seismic Safety Council, "NEHRP Recommended Provisions for the Development of Seismic Regulations for New Buildings," Washington, D.C., (1988).

[2] "Uniform Building Code," 1985 Edition, International Conference of Building Officials, Whittier, CA., (1985).

[3] Ishizuka, T., and Hawkins, N.M., "The Seismic Resistance of Concrete Exterior Column-Beam Subassemblages Containing Unbonded Post-Tensioning Tendons," Dept. of Civil Engineering, University of Washington, Seattle, WA, April, (1986).

[4] Tao, X., Stanton, J.F. and Hawkins, N.M., "A Computer Program for the Moment-Curvature Response of Reinforced and Partially Prestressed Concrete Sections," SM 84-2, Dept. of Civil Engineering, University of Washington, Seattle, WA., (1984).

[5] "Building Code Requirements for Reinforced Concrete," ACI 318-83, Appendix A, American Concrete Institute, Detroit, MI., (1983).

[6] "Recommendations for Design of Beam-Column Joints in Monolithic Reinforced Concrete Structure," ACI-ASCE Committee 352, ACI Journal, American Concrete Institute, Detroit, MI., May-June (1985).

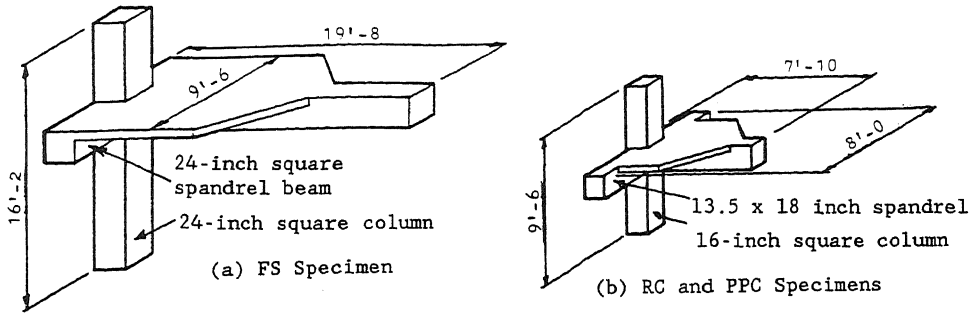

Fig. 1 Specimen Geometry

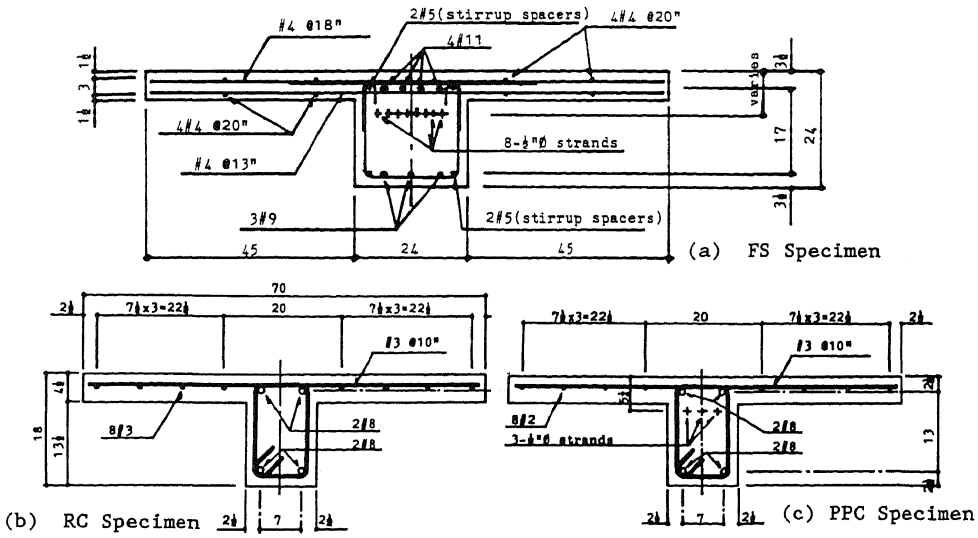

Fig. 2 Beam Cross Sections

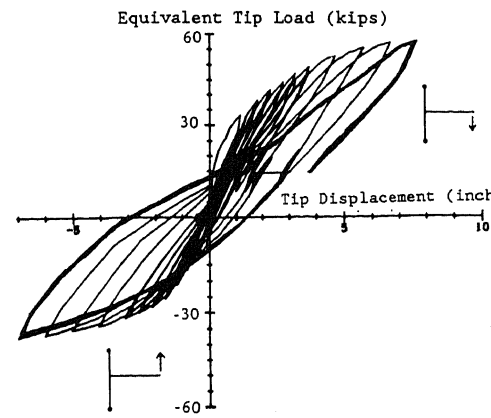

Fig. 3 Equivalent Tip Load-Tip Displacement FS Specimen

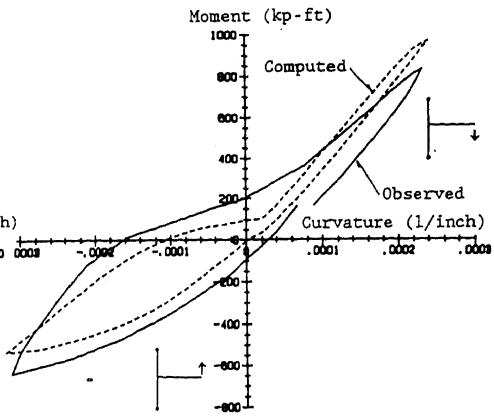

Fig. 4 Measured and Computed Moment-Curvature Relationships - FS Specimen

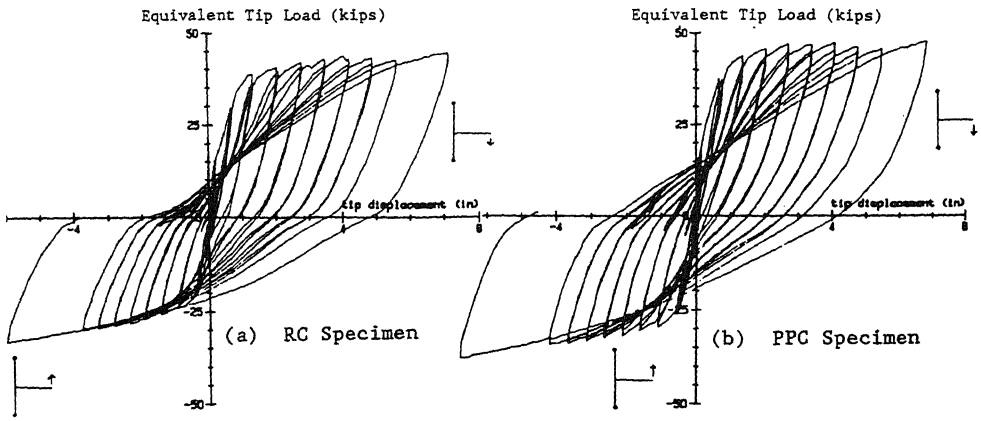

Fig. 5 Equivalent Tip Load-Tip Displacement Relationship

		Specimen	RC	PPC	FS
(1)	downward	μ_w	0.210	0.160	0.163
(2)		μ_{pw}	0.000	0.087	0.053
(3)		$\mu_w + \mu_{pw}$	0.210	0.247	0.216
(4)		$\mu_w/(\mu_w + \mu_{pw})$	1.000	0.650	0.750
(5)	upward	μ_w	0.131	0.126	0.081
(6)		μ_{pw}	0.000	0.034	0.030
(7)		$\mu_w + \mu_{pw}$	0.131	0.160	0.111
(8)		$\mu_w/(\mu_w + \mu_{pw})$	1.000	0.790	0.730
(9)		(7) / (3)	0.640	0.650	0.510

Table 1 Moment Indices

$$\mu_w = A_s f_y/(b_w d f'_c)$$

$$\mu_{pw} = (A_{ps} f_{ps}/(b_w d f'_c)) * (d_p/d)$$

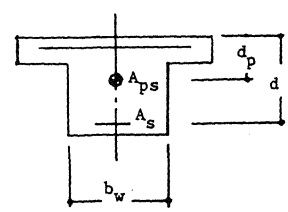

Fig. 6 Moment Index Notation

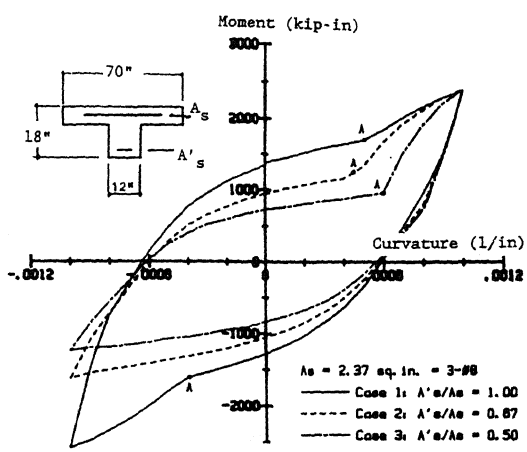

Fig. 7 Effect of A'_s/A_s on Moment-Curvature Relationship

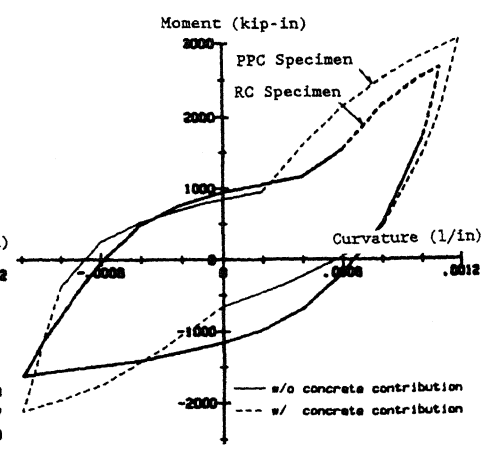

Fig. 8 Predicted Moment-Curvature Relationships - RC and PPC Specimens